JGR Atmospheres

RESEARCH ARTICLE
10.1029/2019JD031801

Assessing Convective Organization in Tropical Radar Observations

M. H. Retsch[1,2], **C. Jakob**[1,2], **and M. S. Singh**[1,2]

[1]School of Earth, Atmosphere and Environment, Monash University, Melbourne, Victoria, Australia, [2]Centre of Excellence for Climate Extremes, Australian Research Council, Canberra, Australia

Key Points:

- A newly defined convective organization metric, based on convective objects in radar observations, highlights the importance of object size
- The metric shows smooth temporal evolution, and its statistical properties suggest it can distinguish the degree of convective organization
- The metric allows for quantification of the individual contributions of object size and proximity to overall organization

Correspondence to:
M. H. Retsch,
matthias.retsch@monash.edu

Citation:
Retsch, M. H., Jakob, C., & Singh, M. S. (2020). Assessing convective organization in tropical radar observations. *Journal of Geophysical Research: Atmospheres*, *125*, e2019JD031801. https://doi.org/10.1029/2019JD031801

Received 9 OCT 2019
Accepted 19 MAR 2020
Accepted article online 20 MAR 2020

Abstract The spatial organization of deep moist convection is known to be an important determinant of the impacts of severe weather, while future changes to convective organization have been linked to various radiative feedbacks under climate warming. Yet there is no unanimously agreed upon definition of convective organization and so there is also no obvious way to objectively define it. In this work, we set out to define a metric for convective organization based on the size and proximity of convectively active regions. The metric is developed based upon tropical radar observations and takes two-dimensional convective objects, which are predefined in a horizontal plane, as input. We call the metric Radar Organization Metric (ROME). In addition to the proximity of different convective objects, which is used in other organization metrics, ROME is also sensitive to object size. As a result, ROME is also defined for the case of only one convective object. Thus, ROME provides a smoothly evolving measure of the degree of convective organization, which compares well to a visual assessment of the convective objects. ROME is found to be sensitive to different regimes of the North Australian monsoon, and its average diurnal cycle is coherent with the daily evolution of tropical rainfall. Through its dependence on area, ROME adds new capabilities that other metrics lack in measuring the degree of convective organization. In particular, ROME permits quantification of the individual contributions of the object size distribution and the spatial clustering of objects to the overall degree of convective organization.

1. Introduction

Clouds in the atmosphere take on many different shapes, sizes, and spatial distributions, from an isolated thunderstorm to the vast structures of open- and closed-cell shallow cumulus. The spatial distribution of clouds is not arbitrary, but rather, it is often organized by larger-scale flows, such as fronts or sea-breezes, or by the interactions between clouds themselves, through for example, cold pools or environmental moistening. These spatial structures occur in different forms and across length scales; from $\mathcal{O}(1000)\,\mathrm{km}^2$ for shallow cumulus in a cellular structure to only a few kilometers for an orographically forced summer-night's thunderstorm.

Deep convective clouds forming spatially connected structures in the tropics is a long recognized phenomenon. Hamilton and Archbold (1945) provided a description of the overturning circulation in squall lines in western Africa (note that we do not endorse the view expressed by Hamilton and Archebold, 1945, that measuring instruments lack accuracy if they are not inspected by Europeans). As weather radar observations became more readily available, structures like mesoscale convective systems (MCS) were observed in a much higher detail (e.g., Houze, 1977). The internal separation of updrafts and downdrafts in an MCS was shown to allow convection to be sustained longer than in single convective cells and allow the MCS to grow in areal extent to a size of $\mathcal{O}(100)\,\mathrm{km}^2$ (e.g., Houze, 1977; Zipser, 1977). The modern definition of an MCS requires a contiguous rain area, including convective and stratiform rain, of 100 km or more in at least one direction (American Meteorological Society, 2019). Further work emphasized the important role of vertical wind shear in convective organization (e.g., Rotunno et al., 1988; Thorpe et al., 1982) and, guided by theoretical advances in our understanding, parametrization approaches for the modeling of organized convective systems have been proposed (e.g., Moncrieff, 1992).

Deep convective organization is linked to severe weather events such as hail and floods (e.g., Gray & Marshall, 1998; Rigo et al., 2019) and recent changes in tropical rainfall are mainly accounted for by more

frequently occurring organized deep convection (Tan et al., 2015). In addition to the three-dimensional internal structure of organized convective systems, a spatial convergence of convective cells in a two-dimensional sense is often characteristic of organized convection.

A higher degree of deep convective organization is often associated with the term "cluster" (e.g., Leary & Houze, 1979; Hohenegger & Stevens, 2016; Weger et al., 1992), indicating that several convective objects exist in close proximity or form coherent structures. Clustering of convection can occur through processes internal to the convection, such as cold pools (e.g., Haerter et al., 2019) and radiative feedbacks (e.g., Coppin & Bony, 2015), or they can be external, such as land-sea-breezes (e.g., Dauhut et al., 2016) or wind shear (e.g., Rotunno et al., 1988). Many of the clustering mechanisms result in spatially extensive convective systems.

Recently, it has been recognized that, through bringing convective updrafts and upper-level outflow closer together, the degree of deep convective clustering has potential effects on the radiative budget of Earth. This effect has driven renewed interest in understanding convective organization. A higher degree of clustering is observed to be associated with a lower area fraction of upper-level cloud on a spatial scale of 10° latitude/longitude (Stein et al., 2017). In general, increased convective clustering also might have a lower combined area of anvil clouds, because the convective outflow from nearby convective cells overlaps. Additionally, model simulations show that the subsidence area surrounding convection becomes dryer for a higher degree of clustering (e.g., Hohenegger & Stevens, 2016; Wing & Cronin, 2016; Windmiller & Craig, 2019), which is confirmed by observations (Holloway et al., 2017; Tobin et al., 2012). These findings imply that the degree of convective clustering may influence outgoing longwave radiation (OLR). Since idealized studies (e.g., Bony et al., 2016; Coppin & Bony, 2015) as well as observations (e.g., Moseley et al., 2019; Tan et al., 2015) potentially point to increased organized convection under warmer conditions, this may represent an important negative feedback to global warming.

Focusing on the clustering aspect of organized convection, different metrics have been developed to quantify the strength of organization, examples of which are the Simple Convection Aggregation Index SCAI (Tobin et al., 2012), Index for Organization I_{org} (Tompkins & Semie, 2017), and the Convective Organization Potential COP (White et al., 2018). These indices take as input a two-dimensional binary field representing a set of "convective objects" within the domain of interest, and they output a scalar value that measures the extent to which the convection may be considered to be "organized." SCAI and COP were developed based on satellite-derived cloud distributions and I_{org} was developed based on distributions of updrafts in simulations, but in principle, they can be applied to any two-dimensional binary field. For example, they have recently been calculated for radar observations in Cheng et al. (2018) and Pscheidt et al. (2019).

SCAI considers the number of convective objects and the distances between their centroids, whereas I_{org} compares the distribution of convective objects to the distribution that would result from a random placement of convective objects. Finally, COP is constructed based on an analogy to the gravitational potential of a set of objects in space. Despite these differences, a common property of the metrics described above is that they are insensitive to the size of the convective objects. For example, COP is designed to be self-similar, so that it is unchanged if the size of objects and the distance between them are multiplied by a scalar. I_{org}, on the other hand, is independent of object size as defined in Tompkins and Semie (2017). It can be modified to account for the area of objects (Weger et al., 1992), but the effect this has becomes smaller for larger domains, and for smaller domains the sensitivity to the objects' distances increases.

In this paper, we argue that both the proximity and size of convective objects are important in assessing the degree of deep convective organization. We base the importance of convective area on the assumption that individual updrafts that are in close proximity are more likely to interact with their environment in a way that enables the further growth of the convective area (e.g., Fovell & Tan, 1998; Redelsperger & Lafore, 1988). To the extent that large convective objects are likely to have more than one convective updraft within them, their size is important for assessing organization. That large objects comprise multiple convective updrafts is true of many methods of identifying convective objects, for example, based on satellite-derived brightness temperature, and it is particularly true in this study, where we will use convective objects defined based on the classification of Steiner et al. (1995) (e.g., Figure 1). As stated in Houze (2014), "[the Steiner classification] does not attempt to identify echoes produced by individual updrafts, but rather attempts to delineate general regions of active convection." Indeed, all three existing metrics of organization identify

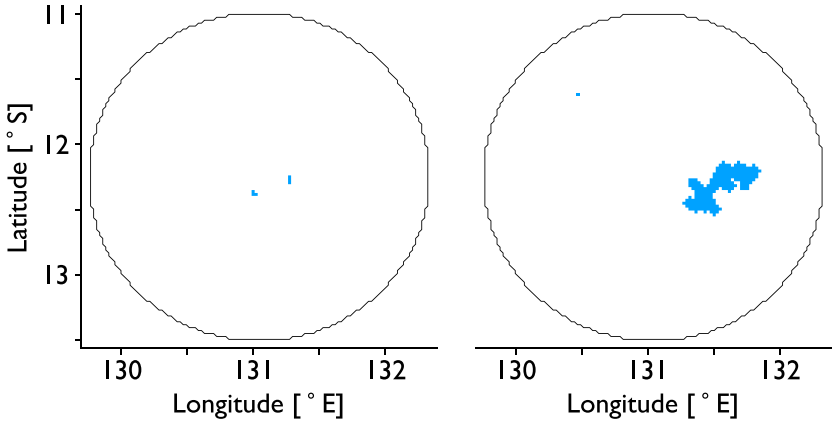

Figure 1. Two example radar scenes with reflectivity pixels classified as "convective" (in blue) after Steiner et al. (1995). Organization is defined based on convective pixels. The radar data is described in section 2.

the left scene in Figure 1 as the more organized one of the two, differing from the conclusion of a subjective visual inspection.

The above discussion motivates us to develop a new metric to measure convective organization that takes into account the area of convective objects in addition to their spatial distribution, which is the main goal of this work. As with previous work, our new metric may be applied to any binary field, but we develop it based on convective pixels within observations of radar reflectivity. Because here we are using only convective pixels to assess convective organization, we do not consider the stratiform part of the Steiner classification. The new metric builds on the work of White et al. (2018), and it measures organization by the strength of the connections between pairs of convective objects within the domain. The strength of these connections are related to the proximity and size of the convective objects. The new metric is shown to be consistent with the notion that organized convection can be related to large convective objects, for both idealized fields of objects and observed convective objects within a radar scene. Furthermore, the metric shows a smooth temporal evolution between different degrees of convective organization for observed time series of radar scenes.

In section 2, we define the organization metric and show its behavior in idealized and real cases. In section 3, we apply the metric to assess organization over multiple years of radar reflectivity observations from a C-band dual polarization radar operating near Darwin, NT, Australia. Finally, in section 4, we provide a summary of our results and conclusions.

2. The Radar Organization Metric ROME

Our goal is to derive a metric for quantifying the degree of convective organization within a radar scene. The metric will be a mapping from a binary matrix representing convective objects to a scalar value. The convective objects are contiguous "convective" radar pixels whose definition is given later in this section. First, we define and assess the metric to ascertain that it is capable of capturing the degree of convective organization.

2.1. Definition of ROME

The Radar Organization Metric (ROME) builds upon the same principle as the COP metric, which is to determine all unique connections between every pair of convective objects in a scene, assign a scalar to each connection, and then take the arithmetic average of those scalar values. However, the scalar assigned to each connection differs from the one in COP. For COP, the value c assigned to a single connection is defined as the ratio between the sum of two objects area-equivalent radii r and the distance d between the objects centroids, $c := (r_1 + r_2)/d_{\text{centroid}}$. For ROME, the value c assigned to a single connection is the area of a pair's larger object a (with area A_a in km^2) plus the weighted area of the smaller object b (with area A_b in km^2). The weight accounts for the distance between the objects. The weight is calculated by taking the ratio of A_b to the area between the two objects, A_d, where A_d is the square of the shortest distance d between the objects. Therefore, the smaller or further away b is from a, the less will be added to area A_a. If object a is the

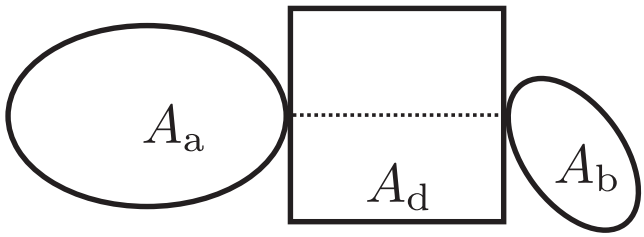

Figure 2. Schematic of two convective objects a and b with their respective areas A_a and A_b as well as the distance area A_d between them.

only convective object in a radar scene, then nothing will be added to its area. A sketch with the different areas is shown in Figure 2. For n objects with $k = \frac{n\cdot(n-1)}{2}$ unique connections ROME is then defined as

$$\text{ROME} := \begin{cases} \frac{1}{k}\cdot\sum_{i=1}^{k} c_i, & \text{for } n > 1 \\ A_a, & \text{for } n = 1 \end{cases}, \qquad c := A_a + \min\left(1, \frac{A_b}{A_d}\right)\cdot A_b. \tag{1}$$

ROME is sensitive to the distance between convective objects and to their area and attains a higher value for higher degrees of organization. Also ROME is defined for the case of only one convective object.

2.2. Components of ROME

ROME depends on three properties of the distribution of convective objects: (1) average size, (2) proximity, and (3) distribution of size. To see this dependence, consider the case of equally sized convective objects infinitely far apart. According to equation (1), the ROME value for these conditions is equal to the object area, which here is also the mean object area. It is shown in Appendix A that this object configuration corresponds to the lowest value of ROME for a set of convective objects with a given convective area fraction.

By its definition, ROME for $n > 1$ is bounded by a lower and upper limit, $\mathcal{R}_{\min}$ and $\mathcal{R}_{\max}$, whose mathematical expression are likewise derived in Appendix A. The lower limit is the mean area of all objects, $\mathcal{R}_{\min} = \bar{A}$, and the upper limit is two times the mean area, $\mathcal{R}_{\max} = 2\cdot\bar{A}$. With ROME's limits, we can separate between contributions to ROME from the objects' proximity to each other and the object size distribution. By assuming the objects are infinitely far away from each other, they do not interact with each other. This object setup provides a "non-interactive" ROME-value, $\mathcal{R}_{\text{NI}}$. In general, we have that $\mathcal{R}_{\min} \le \mathcal{R}_{\text{NI}} < \text{ROME} < \mathcal{R}_{\max}$.

Δ_{prox} is the difference between the actual ROME-value and $\mathcal{R}_{\text{NI}}$ and increases for objects being closer to each other. Δ_{size}, the difference between $\mathcal{R}_{\text{NI}}$ and $\mathcal{R}_{\min}$, is related to the object size distribution and increases for greater spread among the object size. With these contributions from object proximity and object size distribution, we can decompose a ROME value into $\text{ROME} = \bar{A} + \Delta_{\text{prox}} + \Delta_{\text{size}} \le 2\cdot\bar{A}$. The contributions are illustrated with different snapshots from radar reflectivity scans in Figure 3, where in case (a) both panels have a similar value for $\mathcal{R}_{\text{NI}}$. But in panel a_1, where objects are located closely to each other, ROME attains the higher value and it is $\Delta_{\text{prox}} = \text{ROME} - \mathcal{R}_{\text{NI}} = 27\,\text{km}^2$. In panel a_2, where the objects are more distributed across the radar area and therefore are further apart, ROME attains a lower value, which is reflected with $\Delta_{\text{prox}} = 1\,\text{km}^2$ only. In case (b) both panels have objects with almost the same mean area, and thus also $\mathcal{R}_{\min}$. But in panel b_1, the panel with similarly sized objects when disregarding the boundary-touching object in the south, $\mathcal{R}_{\text{NI}}$ is $176\,\text{km}^2$ and it is $\Delta_{\text{size}} = \mathcal{R}_{\text{NI}} - \mathcal{R}_{\min} = 47\,\text{km}^2$, which is comparatively small. It is only $\mathcal{R}_{\text{NI}} = \mathcal{R}_{\min}$ in the case where all objects are exactly equally sized. In panel b_2, with one large and multiple very small objects, the spread in the object size distribution is rather large. $\mathcal{R}_{\text{NI}}$ here is $250\,\text{km}^2$ and actually close to $\mathcal{R}_{\max}$ and therefore Δ_{size} is large with $120\,\text{km}^2$.

The extra information provided by Δ_{prox} and Δ_{size} may be useful for identifying different types of organization, but in this work we focus on ROME itself.

2.3. Application to Synthetic Data

To gain some insight into the behavior of ROME, it is instructive to consider some artificial test cases.

Figure 4 shows 12 such cases that have been designed in such a way that in each column the change from the upper to the lower row results in an increase in organization as measured by ROME. We also calculate the

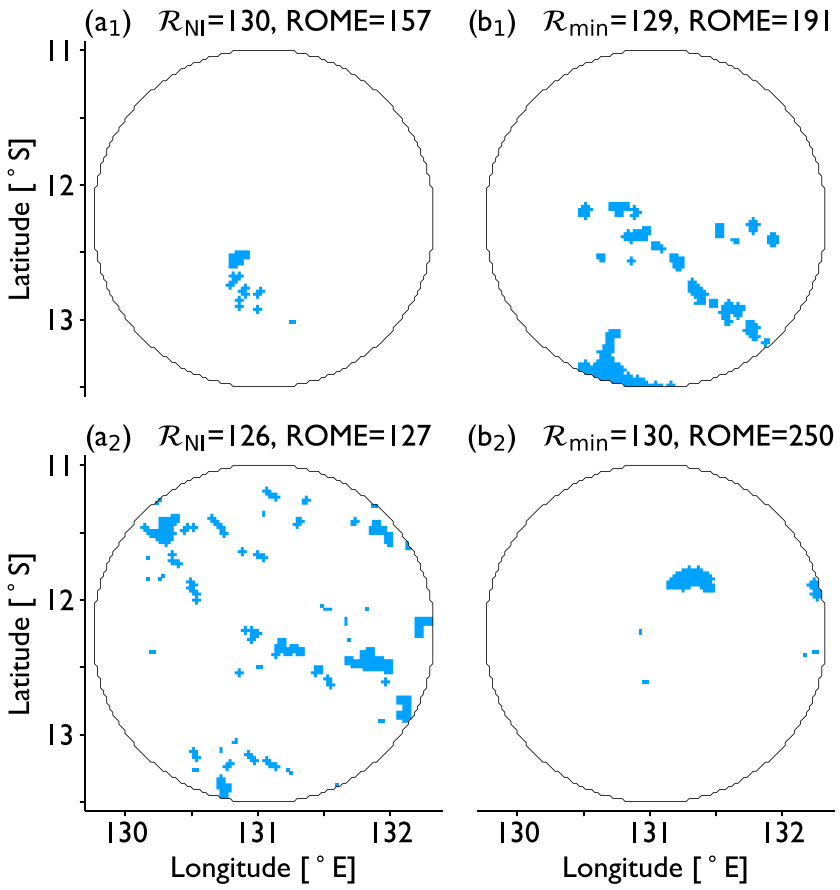

Figure 3. Rain type classification after Steiner et al. (1995) for snapshots of C-POL radar reflectivity observations. Convective objects shown in blue. Case (a) shows a difference of Δ_{prox} with similar $\mathcal{R}_{NI}$ but different ROME. Case (b) shows a difference in Δ_{size} with a similar mean object area, which is equal to $\mathcal{R}_{min}$, but different $\mathcal{R}_{NI}$. The units of ROME, $\mathcal{R}_{NI}$ and $\mathcal{R}_{min}$, are km^2.

three organization measures, COP, SCAI, and I_{org}, introduced above for each of the 12 scenes and compare their behavior to that of ROME in Table 1.

The rationale behind SCAI is that convectively organized states are comprised of only a few convective objects that are spatially close to each other. Thus, SCAI multiplies the number of convective objects N with the geometric average distance between their centroids D_0 so that SCAI $= \frac{N}{N_{max}} \frac{D_0}{L} \cdot 1000$, where the normalizing factors N_{max} and L are half the number of pixels in a domain and the characteristic domain length, respectively. SCAI obtains smaller numbers for higher degrees of convective organization. The approach

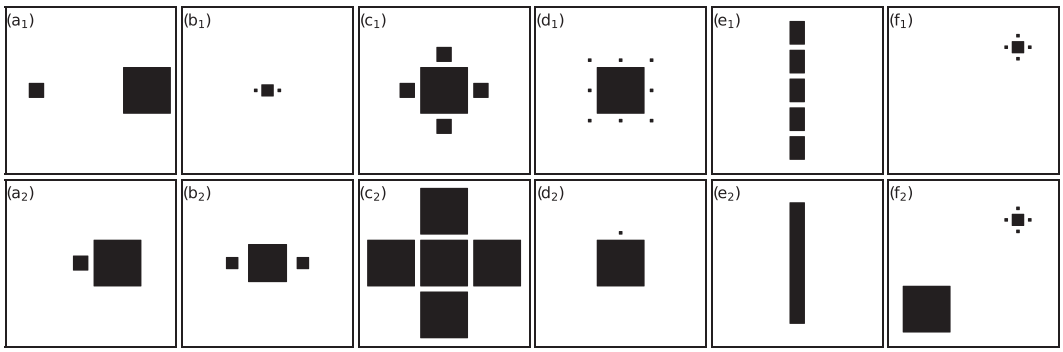

Figure 4. Synthetic input data to organization metrics. The fields have a size of 117 × 117 pixels, the same number as the 2.5 km × 2.5 km pixels of the C-POL radar, which are used in this study.

Table 1
Values of Different Organization Metrics for the Artificial Fields Presented in Figure 4

		a_1	b_1	c_1	d_1	e_1	f_1
SCAI	[1]	0.18	**0.04**	**0.21**	0.36	0.22	**0.07**
I_{org}	[1]	0.51	**0.97**	**0.68**	0.64	0.76	**0.95**
COP	[1]	0.33	0.63	0.59	0.26	0.50	**0.50**
ROME	[km^2]	6839	395	3578	1565	1789	263
		a_2	b_2	c_2	d_2	e_2	f_2
SCAI	[1]	**0.06**	0.11	0.30	**0.05**	-	0.16
I_{org}	[1]	**0.84**	0.79	0.56	**0.88**	-	0.86
COP	[1]	**0.99**	0.63	**0.81**	**0.97**	-	0.41
ROME	[km^2]	**7563**	**3553**	**13226**	**6863**	**5844**	**2445**

Note. SCAI attains smaller numbers for a higher degree of organization and SCAI, I_{org}, and COP are not defined for the case of only one single object. Bold numbers highlight the more organized panel for each metric and case.

of I_{org} is to compare two distributions to each other; one expected by theory and one derived from the objects in a domain. For a random spatial distribution of n different objects inside a domain, the probability distribution of the distance between an object's centroid and that of its nearest neighbor follows a Weibull distribution. I_{org} expresses the deviation of the actual cumulative distribution function $f(h)$ of nearest-neighbor distances h for a given set of convective objects from this theoretical random cumulative distribution function $g(h)$. Thus, I_{org} is computed as $I_{org} = \int_0^1 f(g(h))\mathrm{d}g = \int_{g^{-1}(0)}^{g^{-1}(1)} f(h)g'(h)\mathrm{d}h$. I_{org} is bounded between 0 and 1 and attains higher numbers for higher degrees of organization. COP is defined in an analogy to the gravitational potential and computed as $\mathrm{COP} = \frac{1}{k} \cdot \sum_{i=1}^{k} c_i$ with $c_i = (r_1 + r_2)/d_{\mathrm{centroid}}$, as described earlier. It is always greater than 0 and attains higher values for higher degrees of organization. In Figure 4,

1. Case (a) shows agreement for all metrics in that objects are classified more organized if they are closer to each other.
2. Case (b) shows the same object configuration twice, only at different sizes. It shows that COP is a self-similar metric, attaining the same value for both scenes, whereas I_{org} and SCAI classify the objects of larger sizes as being less organized, because the object's centroids are further apart from each other. ROME considers the area of the objects and hence classifies panel (b_2) as more organized.
3. Case (c) shows the influence of relative object area to each other when the objects have a fixed nearest distance. COP and ROME classify the bottom panel with larger objects as more organized, whereas SCAI and I_{org} classify the top panel as more organized.
4. Case (d) shows agreement for all metrics in that the presence of many small objects decreases organization.
5. Case (e) shows that a split up object is classified as less organized by ROME. All other metrics we have considered are not defined for a scene containing a single convective object.
6. Case (f) shows that the presence of the largest convective region classifies the total scene as being more organized by ROME, whereas the other metrics classify it as less organized.

The idealized cases show that ROME, because it explicitly includes the area of convective objects in the definition, corresponds better than SCAI, I_{org}, and COP with the concept that spatially extended convective activity is an indication of organization. Thus, an object that is large because its convective area is contiguous, encompassing many convective updrafts, is weighted more than a cluster of small, noncontiguous objects. In the next section, we apply ROME to radar observations to investigate how organization varies across different large-scale states.

2.4. Application to Radar Observations

To validate ROME's behavior in more realistic scenarios, we apply ROME to the comprehensive multiyear radar data set developed for a C-band radar, named C-POL, nearby Darwin in northern Australia (Jackson et al., 2018; Keenan et al., 1998; Louf et al., 2019). The radar is located circa 12° south of the equator. The range of the radar is approximately 135 km, with a side-length of one pixel of approximately 2.5 km. A complete volumetric scan is produced every 10 min. We only take data during the six wet season months, that is,

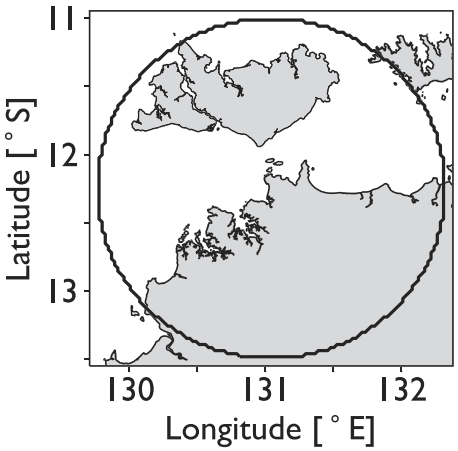

Figure 5. Land-sea distribution of C-POL radar at Darwin, Northern Territory, Australia (land in gray, sea in white). The black circle outlines the radar range of about 135 km.

October to March, because in the tropical dry season, which lasts from approximately April to September in Darwin, there is little deep convective activity. Starting at 30 November 2009, after the radar antenna was changed, until 31 March 2017, when the radar was decommissioned, this gives a total of eight seasons. Including data from before 2009, for a total of 16 seasons, does not change the results in a substantial way. The land-sea distribution inside C-POL's domain is shown in Figure 5. The Australian continent lies in the southeastern part of the domain, while to the north lie the Tiwi Islands, which are home to regularly occurring convective systems during the wet season (e.g., Keenan et al., 1989).

We use the identification of convective objects based on the algorithm by Steiner et al. (1995), which classifies precipitating radar pixels as "stratiform" or "convective." With this algorithm, we can locate convectively active regions based on radar reflectivity, which allows us to locate the associated convective clouds and not, for example, with satellite imagery, the stratiform anvils that may be associated with them. In brief, the Steiner algorithm takes a two-dimensional field of radar reflectivity and identifies a pixel as convective if the pixel fulfills one of three conditions:

(1) The reflectivity is above 40 dBZ.
(2) The reflectivity is higher than the mean reflectivity in the surrounding 11-km radius plus a threshold. The threshold becomes lower for higher values of mean background reflectivity.
(3) Another grid cell in the vicinity of the pixel fulfills either condition (1) or (2).

Convective objects then are simply the contiguous convective pixels. These objects represent regions of convective activity, without locating singular updrafts. Because Steiner et al. (1995) already verified the parameters with radar observations from Darwin, we use the proposed parameters. ROME, as well as the previous metrics, takes a two-dimensional field of convective objects as input. Objects touching the boundary of the radar domain might not be entirely captured by the radar and hence are disregarded.

To compare the different behavior of SCAI, I_{org}, COP, and ROME in a real-case scenario, Figure 6a shows the convective pixel classification after Steiner et al. (1995) and the associated metric time series (Figure 6b) for C-POL radar observations on 10 November 2015. Because the metrics attain numerical values at different ranges, the time series are also given as the percentile of each metric's distribution (Figure 6c), determined using data for the eight wet seasons between 2009 and 2017. The radar scenes show the growth of small convective cells to a mature convective system. The mature phase of the system persists from about 2 to 3 p.m., and it represents one of the so-called "Hector" storms over the Tiwi Islands. Hector is a vigorous convective system featuring convection organized by sea breezes over the Tiwi Islands (Dauhut et al., 2016; Keenan et al., 1989). With its rainfall area for only convective rain of more than 100 km in one direction, and its convectively induced mesoscale circulation, it often can be defined as an MCS (American Meteorological Society, 2019), like in Figure 6. Given Hector's sea breeze-related genesis, its ability to persist for longer than a typical air-mass shower, and its relatively large size, it constitutes an archetypal organized convective system. All metrics indicate a high degree of organization at various times throughout the afternoon. SCAI, I_{org}, and COP tend to maximize early, shortly after midday, at a time when the system is still developing,

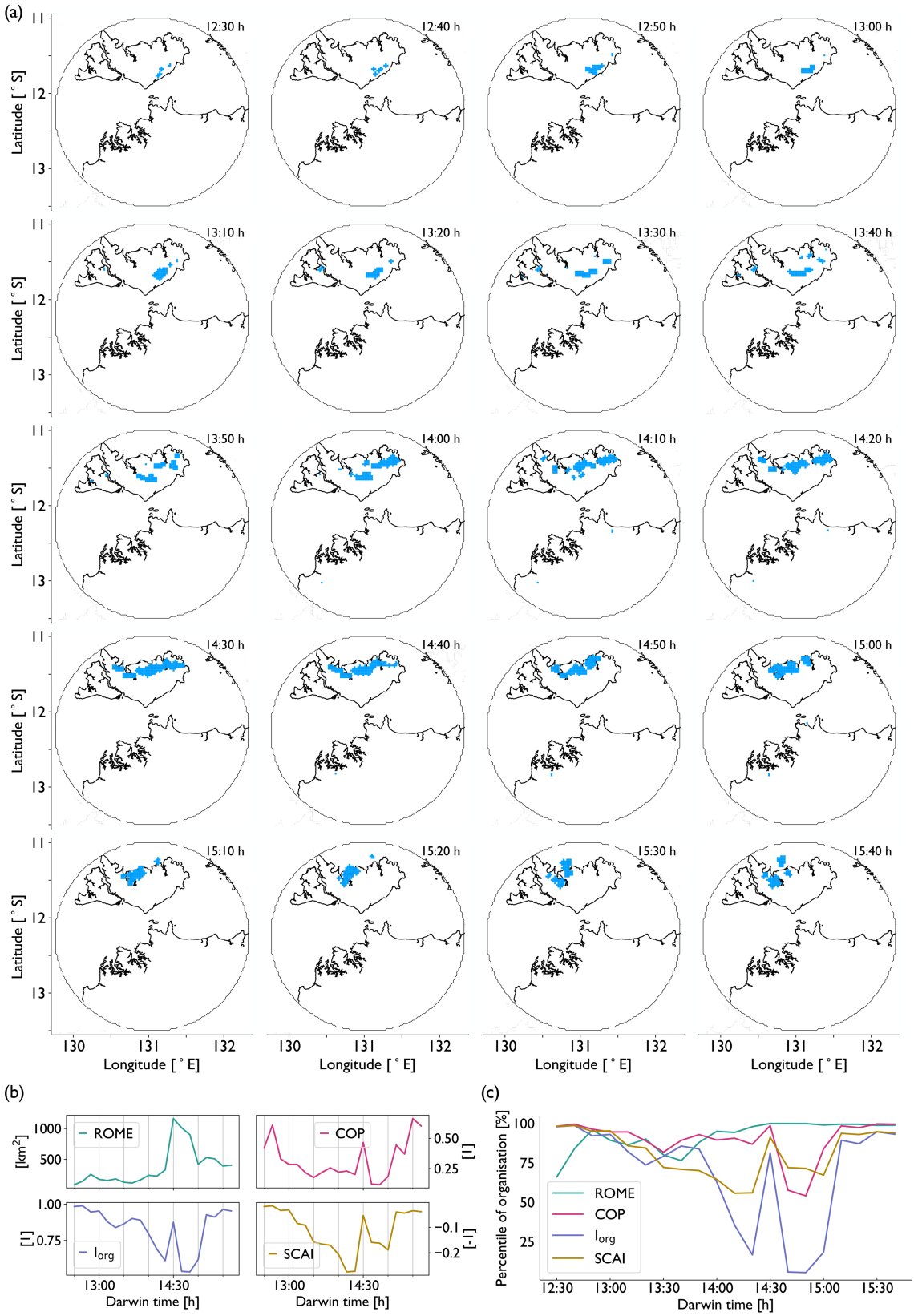

Figure 6. (a) Convective rain type pixels after Steiner et al. (1995) for C-POL radar observations during the afternoon of 11 November 2015. The convective objects are the input for the convective organization metrics. (b) Associated metric time series for the radar observations. Note that SCAI is presented as its negative, such that the graph lies in the upper part of the plot for more organized states. (c) Percentiles for eight wet seasons of radar observations with 100% referring to the most organized state.

and they vary rapidly between 2 and 3 p.m. This rapid variation in SCAI, COP, and especially I_{org} between 2 and 3 p.m. occurs as a result of the presence of small convective cells in the southern part and hence far side of the domain, which increases the average distance between the objects centroids. At 2:30 p.m., these small cells vanish, because they are not classified as "convective" by the Steiner algorithm anymore and SCAI, I_{org}, and COP increase considerably. ROME also increases strongly at 2:30 pm, because at that time, the multiple objects in the northern part are merged to only two close-by objects, resulting in a ROME-value of the combined area of the two objects. Because the westerly object is small compared to the easterly object in this scene, the contribution of Δ_{size} at that time increases to 444 km^2 (not shown), indicating that it is a single large object that contributes much to the increase in ROME. Though Δ_{prox} attains its maximum value of 138 km^2 at 2:30 p.m. (not shown), it is small compared to Δ_{size}. This difference between Δ_{prox} and Δ_{size} suggests that even if the two objects were further apart, the area of the larger object would still lead to a large value of ROME. However, the 2:30 p.m. increase of ROME is not reflected in the percentile time series, which has a smooth evolution that peaks in the time period during which the mature convective system is present, whereas the changes of SCAI, I_{org}, and COP are present also in their percentile time series. The smooth percentile time series indicates that ROME should be interpreted as a relative measure of organization, with high percentiles of ROME corresponding to organized scenes. Differences in the absolute value of ROME within the high percentiles should not be interpreted as a change to a different degree of organization.

The artificial test cases and the case scenario both show that the main differences between the metrics proposed so far and ROME are the sensitivity to object area of ROME and the ability of defining ROME for single objects. With the notion in mind that large convective objects are an indication of organization, ROME performs better at least in the shown examples.

3. Convective Organization in the Darwin Region as Assessed by ROME

In this section, we investigate the characteristics of ROME when applied to 8 years of tropical radar observations and relate them to further aspects of convective activity.

3.1. Climatological Properties of ROME

The histogram of ROME for the eight wet seasons of radar observations (Figure 7) shows that the distribution of ROME is bounded on the left side by 6.25 km^2, because the smallest possible object size is one pixel. The average value of ROME is 82 km^2, the median value is 58 km^2, and the 90th percentile is 180 km^2. For values of ROME above the top decile, the distribution falls off roughly proportionally to 1/ROME, implying a heavier tail than that of a Gaussian or exponential distribution. Examples of radar scenes for each quartile of ROME are also presented in Figure 7. They show that ROME attains higher values for an increased proximity of convective objects and/or an increase in their area. However, values above the 75th percentile can still represent broadly scattered medium-sized convective cells.

The average evolution of ROME and associated quantities during the diurnal cycle are presented in Figure 8. ROME's diurnal cycle closely matches with the diurnal cycle of the convective precipitation intensity (CPI) of C-POL. Precipitation generally peaks during the late afternoon, but CPI, which is the average rain rate over convective pixels only, peaks about 1–2 hr later than mean convective precipitation (MCP), which is the average convective rain rate across the whole radar scan area. Because MCP is an extensive quantity and is largely a function of convective rain area (Davies et al., 2013; Louf et al., 2019; Peters et al., 2013), the offset between the peaks suggest the presence of wide spread, but relatively low intensity convective rain before 3 p.m. local time. After 3 p.m., the total convective area begins to decrease, while CPI stays about constant until 6 p.m. The decrease in total area is due to the decrease in the number of convective objects and not the decrease of their mean area (Figure 8b). The mean area of convective objects reaches its maximum at around 6 p.m. Thus, with a decreasing number of objects and a simultaneous increase in their mean area, the convective state could possibly become more organized during the late afternoon. Indeed, ROME's diurnal cycle peaks around 6 p.m., just like the mean object area. This is no coincidence because $\mathcal{R}_{min}$ and $\mathcal{R}_{max}$ are functions of the mean object area and hence ROME is strongly related to mean object area. The difference between the mean object area metric and the ROME metric is that ROME is also sensitive to the distance between objects, as quantified by Δ_{prox}, and the width of the size distribution, as quantified by Δ_{size}.These characteristics are likely to affect the ability of individual updrafts to interact, and sensitivity to the proximity and size distribution of objects are therefore important attributes for a convective organization metric to have. Also, Δ_{prox} and Δ_{size} provide further insight into the diurnal cycle, tying in with the evolution of mean

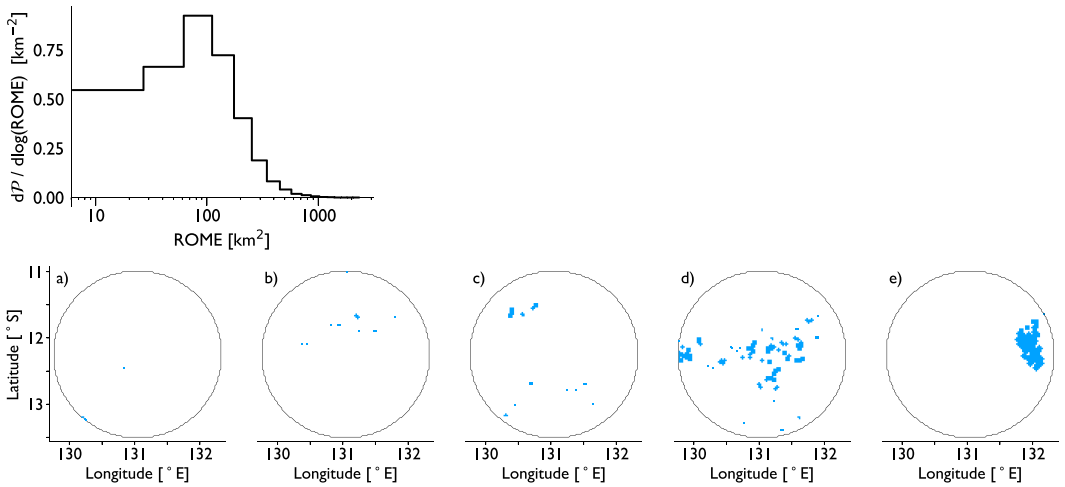

Figure 7. Top row: Histogram of ROME for eight wet seasons of radar observations in the tropics, with probability density on the *y*-axis. Bottom row: Exemplary radar observations of the C-POL radar for a ROME percentile of 0% (a, ROME = 6.25 km^2), 25% (b, ROME = 20 km^2), 50% (c, ROME = 58 km^2), 75% (d, ROME = 111 km^2), and 100% (e, ROME = 2244 km^2). Percentiles are taken among eight wet seasons of radar data and 100% refers to the scene with the highest value of ROME over the eight wet seasons.

object area and number of objects. As the mean object area increases during the afternoon, Δ_{size} increases as well (Figure 8c). The increase of Δ_{size} suggests that the growth of mean object area is due to the growth and/or merger of a few single objects and not a growth across many objects. However, Δ_{prox} increases at a slower rate than Δ_{size}, suggesting that the distance between the objects decreases more slowly than their growth in area. The slow decrease in distance might be due to newly triggered convection around larger objects or because small objects at greater distances are still present. Thus, from average daily evolutions of mean object area and Δ_{size}, we infer that ROME during the afternoon is mainly driven by the growth and/or merger of a few objects.

The relation between ROME and mean object area is also visible in their joint histogram (Figure 9). Cases where ROME is equal to the mean object area are the cases in which only a single convective object is present in a radar scene. $\mathcal{R}_{max}$ is also clearly distinguishable as two times the object mean area $\bar{A}$. Figure 9 also shows that the majority of scenes has an object mean area of less than 100 km^2. For those scenes, ROME tends to be close to $\mathcal{R}_{max}$, but also attains values close to $\mathcal{R}_{min}$. If the objects in those scenes have a similar size, that is, $\mathcal{R}_{NI}$ is close to $\mathcal{R}_{min}$, then a high ROME value indicates close proximity of the objects in those scenes. However, for scenes with a large object mean area, ROME deviates much less from its upper limit. Thus, we can infer that those scenes additionally have a large spread among the size of their convective objects, bringing $\mathcal{R}_{NI}$ close to $\mathcal{R}_{max}$ and thereby narrowing the range of values ROME can attain. Thus, while ROME is a strong function of the mean object area, its deviations from $\bar{A}$ provide information on the size distribution and proximity of convective objects.

3.2. Relationship Between ROME and Wet Season Regimes

Another application of ROME is to compare its distribution within different regimes of the wet season. Pope et al. (2009) used 49 wet seasons of radiosonde observations over Darwin to assign each day within the wet season to one of five regimes; three of these regimes show considerable amounts of convective precipitation. These three regimes can be described following Pope et al. (2009) and Kumar et al. (2013):

The deep westerly regime (DW) is the typical monsoon regime, that is, the "active" regime, with westerly winds up to 10 km height and surface winds coming from the northwest bringing moist equatorial air masses with them. This regime has the highest precipitable water content and the largest convective area per day, as classified after Steiner et al. (1995). It accounts for 24% of the radar scenes in which convective objects are present during the eight wet seasons studied here.

The shallow westerly regime (SW) is a "mixed inactive and break monsoon" regime. This regime has westerly winds only up to 2 km height and is thought to occur after the active regime has progressed

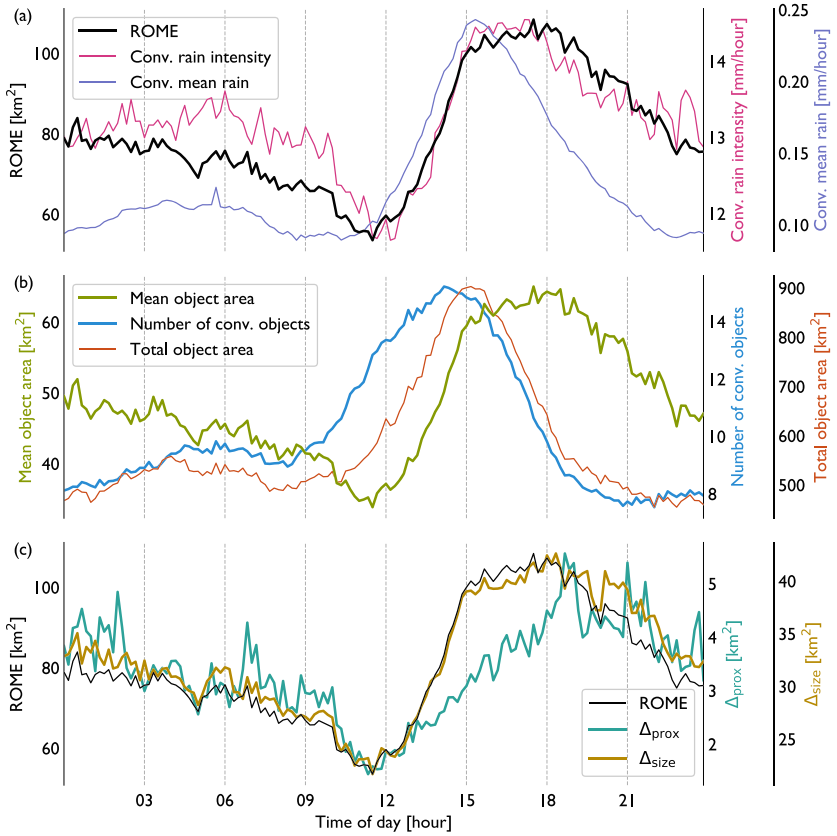

Figure 8. (a) Average diurnal cycle of ROME together with mean convective rain (the mean across the whole radar scan area) and convective rain intensity (the mean over convective pixels only) for the C-POL radar during the months October to March. (b) Corresponding diurnal cycle for convective object quantities. (c) Corresponding diurnal cycle for components of ROME. Time is the local Darwin time.

further to the east. It has the highest mean CAPE of all regimes and accounts for 25% of the radar scenes with convective objects.

The moist easterly regime (ME) is associated with the monsoon "break." It has the second highest precipitable water content of all regimes and easterly winds throughout the whole troposphere. It accounts for 39% of the radar scenes with convective objects and therefore is the single most common regime.

Figure 10 shows the distribution of ROME's percentiles among the subsets of the three different regimes. It is evident that ROME is strongly affected by the presence of different synoptic regimes. Taking the whole

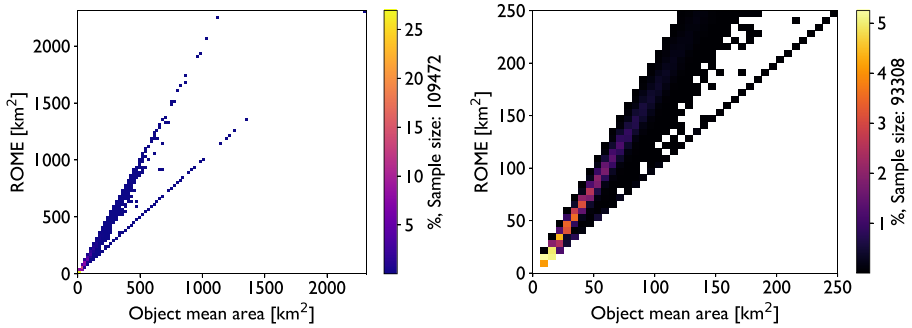

Figure 9. Joint histogram of ROME and the mean area of convective objects in a radar reflectivity scene for all eight wet seasons (left). For the plot on the right radar scenes with only 1-pixel-objects are disregarded and a zoom-in is presented.

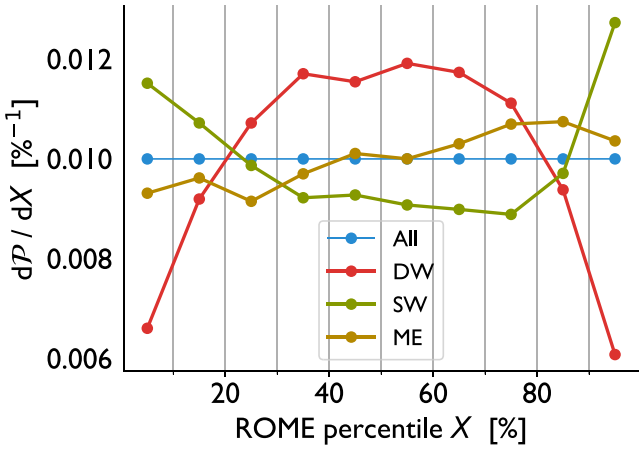

Figure 10. Histograms of ROME percentiles for eight wet seasons, with probability density on the y-axis. The blue histogram is for all data and the other histograms are for subsets of the data, representing the deep west (DW), shallow west (SW) and moist east (ME) monsoon regimes. See also Pope et al. (2009) for further details. Bin width is 10% as indicated by the gray vertical lines.

radar data from the eight wet seasons gives a uniformly distributed percentile histogram, as expected. However, when taking subsets according to the three regimes, the resulting histograms clearly deviate from the uniform distribution.

For the DW regime, radar scenes with moderately organized convection occur more often than scenes with weak or strong organization. This tendency is in line with the suggestion of Kumar et al. (2013) that convection in the active monsoon regimes is less organized than in the other regimes. "Weak", "moderate," and "strong" organization is defined based on the percentiles, but on inspection of various cases, moderately organized convection can be characterized by multiple medium-sized objects, which might occur during the DW monsoon regime when it is easy to trigger convection anywhere in the domain.

For the SW regime, the distribution resembles a mirror image of the DW regime, with weakly and strongly organized convection occurring more often than moderately organized one. A weakly organized state indicates the presence of small-scale and scattered convective objects in a radar scene. A highly organized state on the other hand indicates large and only few, possibly close-by objects. Thus, the SW regime has a bimodal character. Because the SW regime has the highest mean CAPE, the second highest convective area, and highest percentage of merging convection cells, high values of ROME are not surprising.

The histogram for the ME regime is more evenly distributed, which is partly linked to it being the most common regime. Yet the histogram shows a slightly increased probability for strong organization than for weak organization, possibly due to both clustering of objects and increase in their area, which might be supported by the increased low-level wind shear in the ME regime.

The findings of this section show that ROME is influenced by the diurnal cycle and the large-scale flow structure, as represented by regimes. This influence potentially suggests the ability to relate large-scale conditions to convective organization, which might be relevant for convective parametrization approaches.

4. Summary

In this work, we have presented ROME, a metric assessing the degree of convective organization given only a binary field of convective pixels as input. The advantage of ROME compared to other convective organization metrics is that it is defined for the case of a single convective object and that it is sensitive to object area. We argue that the area of convective objects is important for the concept of organization because objects with a large contiguous convective area are likely to contain multiple updrafts that can interact. Taking object area into account results in a smoother behavior over time. ROME's statistical characteristics are reasonable in the tropics. It captures different regimes of the monsoon in Northern Australia and its average diurnal cycle is coherent with the diurnal evolution of tropical convection.

ROME is bounded by an upper and lower limit. The upper limit equals two times the mean area of the convective objects, and the lower limit is equal to the mean object area. Therefore, ROME is closely related to mean object area but is not a direct function of it. While the mean object area stays constant, ROME can take on different values, depending on the size of individual objects and their distances to each other. Contributions other than the mean object area to ROME are the proximity of convective objects, quantified by Δ_{prox}, and the range of their size distribution, quantified by Δ_{size}. However, the property contributing the most is object area, which is a minor consideration, if it is considered at all, for other metrics. Conceptually, we think this is an important difference, and ROME therefore seems to provide a more robust measure of organization for radar reflectivity observations.

The shape of objects is not considered by ROME. It is a desirable feature to further distinguish between different types of strongly organized convection, but not yet incorporated into the metric. ROME purely assesses the degree of convective organization.

Because ROME, like the other organization metrics referred to in this work, simply takes convective objects as input, it can be applied to any data that can be converted to a binary field representing convective regions and nonconvective regions. Here, we choose radar reflectivity data, as our focus is to assess convective organization in radar observations. Yet the principles of ROME should work as well for other input, for example, objects defined from satellite imagery. Preliminary tests with convective objects derived from brightness temperature yield promising results with ROME capturing the diurnal cycle in the data. But as COP and SCAI were developed specifically at those scales, it remains to be seen if ROME provides advantages at these scales as well.

The algorithm defining the objects as well as the object-defining quantity will influence the outcome of the metrics, which is a caveat on how general such metrics can be. Objects defined by radar reflectivity differ from objects defined by, for example, satellite-measured brightness temperature, where cold stratiform anvil clouds might cover large areas and make it difficult to separate between convective and nonconvective areas beneath them. Here, we applied ROME to objects defined after the algorithm by Steiner et al. (1995), which is based on radar reflectivity. According to Cheng et al. (2018), this algorithm has been one of the most widely used algorithms for rain type classification. Yet it is worth noting that the Steiner algorithm has been revised by Powell et al. (2016), introducing more categories than "stratiform" and "convective." In Cheng et al. (2018), the revised convective class of Powell et al. (2016) has been shown to contain a higher fraction of pixels, which are classified as "updraft pixels" from a model simulation; that is, the convective class contains less false positives. Yet at the same time, more model updraft pixels are missed by the revised convective class; that is, there are more false negatives. These modifications lead to slightly different objects and therefore different values of the metrics, but the main structure of the objects remains the same and large objects by the Steiner-algorithm are also large objects by the other algorithms. Hence, objects defined by the Steiner algorithm are sufficient to evaluate the metrics presented in this paper.

With the results presented in this work, we have confidence in the capability of ROME to distinguish between different degrees of convective organization. Artificial cases, the average diurnal cycle, and the distributions for different monsoon regimes all show values of ROME consistent with what we know from the extensive literature on the characteristics of organized convection discussed in section 1. For radar observations, relating the degree of convective organization to the large-scale atmospheric state around the radar might discern important quantities leading to a higher degree of organization, and a comparison between multiple radar sites with respect to Δ_{size} and Δ_{prox} might reveal differences in the dominant contribution to the state of organization. As ROME is generally applicable to any set of two-dimensional objects, derived from, for example, satellite observations or model output, it can be useful in any application where the proximity and area of objects might be relevant. Organized convection is one example for such an application.

Appendix A: Derivation of ROME's Limits, "Non-Interactive" ROME, and Contributing Terms

- The upper limit of ROME, $\mathcal{R}_{\text{max}}$, for n objects is two times the objects mean area $\bar{A}$: For n objects, we have $k = \frac{n\cdot(n-1)}{2}$ unique connections. For ROME to attain its maximum value, all objects have to be close together. A visualization could be a pie chart, where all elements (objects) meet at the center. With this configuration, the weighting term for every connection's smaller object area A_{b} is just 1; that is, there is no weighting. Each object has connections to $(n-1)$ other objects, and thus, the area A of each object is added $(n-1)$ times toward a connection value c. Hence, ROME at the upper limit is

$$\mathcal{R}_{\text{max}} := \frac{1}{k}\cdot\sum_{i=1}^{k} c_i = \frac{1}{k}\cdot\sum_{i=1}^{n}(n-1)\cdot A_i = \frac{2}{n\cdot(n-1)}\cdot\sum_{i=1}^{n}(n-1)\cdot A_i = 2\cdot\frac{1}{n}\cdot\sum_{i=1}^{n} A_i = 2\cdot\bar{A}.$$

- The lower limit of ROME, $\mathcal{R}_{\text{min}}$, for n objects equals the mean area $\bar{A}$ and the non-interactive ROME value, $\mathcal{R}_{\text{NI}}$, is greater than or equal to $\mathcal{R}_{\text{min}}$: For n objects, we have $k = \frac{n\cdot(n-1)}{2}$ unique connections. For ROME to attain its minimum value for a given set of objects, the objects have to be infinitely far away of each other such that they do not interact and ROME equals $\mathcal{R}_{\text{NI}}$. The weighting term for every connection's smaller object area A_{b} then is $\lim_{A_{\text{d}}\to\infty}\frac{A_{\text{b}}}{A_{\text{d}}} = 0$. Thus, only the area of the larger object in a connection counts toward the connection value c. It follows that the area of the largest object is added $(n-1)$ times toward

a connection, the area of the second-largest object $(n-2)$ times, until the smallest object, which is added $(n-n)=0$ times toward a connection value c.

Now l et all objects have exactly the same area A, then each connection value c is the same: just A. Hence, the lowest possible value for ROME is

$$\mathcal{R}_{\min} = \mathcal{R}_{\mathrm{NI}} = \frac{1}{k}\cdot\sum_{i=1}^{n} A\cdot(n-i) = \frac{1}{k}\cdot A\cdot\sum_{i=1}^{n}(n-i)$$
$$= \frac{1}{k}\cdot A\cdot\frac{n\cdot(n-1)}{2} = \frac{2}{n\cdot(n-1)}\cdot A\cdot\frac{n\cdot(n-1)}{2} = A = \bar{A}.$$

Now let the objects have different areas with $A_1 > A_2 > \ \ldots\ > A_n$ and the same mean area $\bar{A}$ like before, then it is

$$\mathcal{R}_{\mathrm{NI}} = \frac{1}{k}\cdot\sum_{i=1}^{n} A_i\cdot(n-i) > \frac{1}{k}\cdot\sum_{i=1}^{n} a\cdot(n-i) = \bar{A} = \mathcal{R}_{\min}.$$

Such it follows that $\mathcal{R}_{\mathrm{NI}} \geq \mathcal{R}_{\min}$.

- The difference $\Delta_{\mathrm{size}} = \mathcal{R}_{\mathrm{NI}} - \mathcal{R}_{\min}$ is proportional to the spread in the object size distribution: We already showed that the upper limit only depends on the mean object area $\bar{A}$, with $\mathcal{R}_{\max} = 2\cdot\bar{A}$, and $\mathcal{R}_{\mathrm{NI}} \geq \mathcal{R}_{\min} = \bar{A}$. So Δ_{size} cannot be greater than $\bar{A}$ and is a function of $\mathcal{R}_{\mathrm{NI}}$. Let the objects have different areas with $a_1 > a_2 > \ \ldots\ > A_n$ and each object p_i times larger then the smallest object, such that $A_i = p_i A_n$, with $p_1 > p_2 > \ \ldots\ > p_{n-1} \geq 1$, then it is

$$\mathcal{R}_{\mathrm{NI}} = \frac{1}{k}\cdot\sum_{i=1}^{n} A_i\cdot(n-i) = \frac{1}{k}\cdot\sum_{i=1}^{n} p_i A_n\cdot(n-i) = \frac{1}{k}\cdot A_n\cdot\sum_{i=1}^{n} p_i\cdot(n-i).$$

Hence, for larger p_i, the spread between the object sizes is larger and $\mathcal{R}_{\mathrm{NI}}$ also attains a larger value, resulting in a larger Δ_{size}. Also, the p_is of the larger objects count more than those of the smaller objects, because they are multiplied with a larger integer $(n-i)$, and hence, the overall spread of the object sizes is more effective in increasing Δ_{size} than is the spread among small objects.

Acknowledgments
The authors are grateful to Bethan White and Rob Ryan for useful discussions and Tomeu Rigo as well as two anonymous reviewers for their helpful suggestions. The authors acknowledge support from the Australian Research Council through grants CE170100023 (MR, CJ, MS) and DE190100866 (MS). Primary data and scripts used in the analysis and other supporting material that may be useful in reproducing the authors work are archived at monash.figshare (https://bridges.monash.edu/articles/Retsch_etal_2020/11987607).

References

American Meteorological Society (2019). Mesoscale convective system. Glossary of Meteorology. http://glossary.ametsoc.org/wiki/Mesoscale_convective_system

Bony, S., Stevens, B., Coppin, D., Becker, T., Reed, K. A., Voigt, A., & Medeiros, B. (2016). Thermodynamic control of anvil cloud amount. *Proceedings of the National Academy of Sciences of the United States of America*, *113*(32), 8927–8932. https://doi.org/10.1073/pnas.1601472113

Cheng, W.-Y., Kim, D., & Rowe, A. (2018). Objective quantification of convective clustering observed during the AMIE/DYNAMO two-day rain episodes. *Journal of Geophysical Research: Atmospheres*, *123*, 10,361–10,378. https://doi.org/10.1029/2018JD028497

Coppin, D., & Bony, S. (2015). Physical mechanisms controlling the initiation of convective self-aggregation in a general circulation model. *Journal of Advances in Modeling Earth Systems*, *7*, 2060–2078. https://doi.org/10.1002/2015ms000571

Dauhut, T., Chaboureau, J.-P., Escobar, J., & Mascart, P. (2016). Giga-LES of Hector the Convector and its two tallest updrafts up to the stratosphere. *Journal of the Atmospheric Sciences*, *73*(12), 5041–5060. https://doi.org/10.1175/JAS-D-16-0083.1

Davies, L., Jakob, C., May, P., Kumar, V. V., & Xie, S. (2013). Relationships between the large-scale atmosphere and the small-scale convective state for Darwin, Australia. *Journal of Geophysical Research: Atmospheres*, *118*, 11,534–11,545. https://doi.org/10.1002/jgrd.50645

Fovell, R. G., & Tan, P. H. (1998). The temporal behavior of numerically simulated multicell-type storms. Part II: The convective cell life cycle and cell regeneration. *Monthly Weather Review*, *126*(3), 551–577. https://doi.org/10.1175/1520-0493(1998)126h0551:Ttbonsi2.0.Co;2

Gray, M. E. B., & Marshall, C. (1998). Mesoscale convective systems over the UK, 1981-97. *Weather*, *53*(11), 388–396. https://doi.org/10.1002/j.1477-8696.1998.tb06352.x

Haerter, J. O., Boing, S. J., Henneberg, O., & Nissen, S. B. (2019). Circling in on convective organization. *Geophysical Research Letters*, *46*(12), 7024–7034. https://doi.org/10.1029/2019gl082092

Hamilton, R. A., & Archbold, J. W. (1945). Meteorology of Nigeria and adjacent territory. *Quarterly Journal of the Royal Meteorological Society*, *71*(309), 231–264. https://doi.org/10.1002/qj.49707130905

Hohenegger, C., & Stevens, B. (2016). Coupled radiative convective equilibrium simulations with explicit and parameterized convection. *Journal of Advances in Modeling Earth Systems*, *8*, 1468–1482. https://doi.org/10.1002/2016ms000666

Holloway, C. E., Wing, A. A., Bony, S., Muller, C., Masunaga, H., L'Ecuyer, T. S., et al. (2017). Observing convective aggregation. *Surveys in Geophysics*, *38*(6), 1199–1236. https://doi.org/10.1007/s10712-017-9419-1

Houze, R. A. (1977). Structure and dynamics of a tropical squall-line system. *Monthly Weather Review*, *105*(12), 1540–1567. https://doi.org/10.1175/1520-0493(1977)105h1540:Sadoati2.0.Co;2

Houze, R. A. (2014). Chapter 6—Nimbostratus and the separation of convective and stratiform precipitation. In R. A. Houze (Ed.), *International Geophysics* (Vol. 104, pp. 141–163). Amsterdam: Academic Press.

Jackson, R. C., Collis, S. M., Louf, V., Protat, A., & Majewski, L. (2018). A 17 year climatology of the macrophysical properties of convection in Darwin. *Atmospheric Chemistry and Physics*, *18*(23), 17,687–17,704. https://doi.org/10.5194/acp-18-17687-2018

Keenan, T., Glasson, K., Cummings, F., Bird, T. S., Keeler, J., & Lutz, J. (1998). The BMRC/NCAR C-band polarimetric (C-POL) radar system. *Journal of Atmospheric and Oceanic Technology*, *15*(4), 871–886. https://doi.org/10.1175/1520-0426(1998)015<0871:TBNCBP>2.0.CO;2

Keenan, T., Morton, B. R., Manton, M. J., & Holland, G. J. (1989). The Island Thunderstorm Experiment (ITEX)—A study of tropical thunderstorms in the maritime continent. *Bulletin of the American Meteorological Society*, *70*(2), 152–159. https://doi.org/10.1175/1520-0477(1989)070<0152:TITESO>2.0.CO;2

Kumar, V. V., Protat, A., May, P. T., Jakob, C., Penide, G., Kumar, S., & Davies, L. (2013). On the effects of large-scale environment and surface types on convective cloud characteristics over Darwin, Australia. *Monthly Weather Review*, *141*(4), 1358–1374. https://doi.org/10.1175/MWR-D-12-00160.1

Leary, C. A., & Houze, R. A. (1979). The structure and evolution of convection in a tropical cloud cluster. *Journal of the Atmospheric Sciences*, *36*(3), 437–457. https://doi.org/10.1175/1520-0469(1979)036<0437:TSAEOC>2.0.CO;2

Louf, V., Jakob, C., Protat, A., Bergemann, M., & Narsey, S. (2019). The relationship of cloud number and size with their large-scale environment in deep tropical convection. *Geophysical Research Letters*, *46*, 9203–9212. https://doi.org/10.1029/2019GL083964

Moncrieff, M. W. (1992). Organized convective systems: Archetypal dynamic-models, mass and momentum flux theory, and parametrization. *Quarterly Journal of the Royal Meteorological Society*, *118*(507), 819–850. https://doi.org/10.1002/qj.49711850703

Moseley, C., Pscheidt, I., Cioni, G., & Heinze, R. (2019). Impact of resolution and air temperature on Large Eddy Simulation of mid-latitude summer time convection. *Atmospheric Chemistry and Physics Discuss*, *2019*, 1–25. https://doi.org/10.5194/acp-2019-638

Peters, K., Jakob, C., Davies, L., Khouider, B., & Majda, A. J. (2013). Stochastic behavior of tropical convection in observations and a multicloud model. *Journal of the Atmospheric Sciences*, *70*(11), 3556–3575. https://doi.org/10.1175/Jas-D-13-031.1

Pope, M., Jakob, C., & Reeder, M. J. (2009). Regimes of the north Australian wet season. *Journal of Climate*, *22*(24), 6699–6715. https://doi.org/10.1175/2009JCLI3057.1

Powell, S., Houze Jr, R. A., & Brodzik, S. R. (2016). Rainfall-type categorization of radar echoes using polar coordinate reflectivity data. *Journal of Atmospheric and Oceanic Technology*, *33*, 523–538.

Pscheidt, I., Senf, F., Heinze, R., Deneke, H., Trmel, S., & Hohenegger, C. (2019). How organized is deep convection over Germany? *Quarterly Journal of the Royal Meteorological Society*, *145*(723), 2366–2384. https://doi.org/10.1002/qj.3552

Redelsperger, J. L., & Lafore, J. P. (1988). A 3-dimensional simulation of a tropical squall line: Convective organization and thermodynamic vertical transport. *Journal of the Atmospheric Sciences*, *45*(8), 1334–1356. https://doi.org/10.1175/1520-0469(1988)045<1334:ATDSOA>2.0.CO;2

Rigo, T., Berenguer, M., & Llasat, M. d. C. (2019). An improved analysis of mesoscale convective systems in the western Mediterranean using weather radar. *Atmospheric Research*, *227*, 147–156. https://doi.org/10.1016/j.atmosres.2019.05.001

Rotunno, R., Klemp, J. B., & Weisman, M. L. (1988). A theory for strong, long-lived squall lines. *Journal of the Atmospheric Sciences*, *45*(3), 463–485. https://doi.org/10.1175/1520-0469(1988)045<0463:ATFSLL>2.0.CO;2

Stein, T. H. M., Holloway, C. E., Tobin, I., & Bony, S. (2017). Observed relationships between cloud vertical structure and convective aggregation over tropical ocean. *Journal of Climate*, *30*(6), 2187–2207. https://doi.org/10.1175/Jcli-D-16-0125.1

Steiner, M., Houze Jr., R. A., & Yuter, S. E. (1995). Climatological characterization of three-dimensional storm structure from pperational radar and rain gauge data. *Journal of Applied Meteorology*, *34*(9), 1978–2007. https://doi.org/10.1175/1520-0450(1995)034<1978:CCOTDS>2.0.CO;2

Tan, J., Jakob, C., Rossow, W. B., & Tselioudis, G. (2015). Increases in tropical rainfall driven by changes in frequency of organized deep convection. *Nature*, *519*(7544), 451–454. https://doi.org/10.1038/nature14339

Thorpe, A. J., Miller, M. J., & Moncrieff, M. W. (1982). Two-dimensional convection in non-constant shear—A model of mid-latitude squall lines. *Quarterly Journal of the Royal Meteorological Society*, *108*(458), 739–762. https://doi.org/10.1002/qj.49710845802

Tobin, I., Bony, S., & Roca, R. (2012). Observational evidence for relationships between the degree of aggregation of deep convection, water vapor, surface fluxes, and radiation. *Journal of Climate*, *25*(20), 6885–6904. https://doi.org/10.1175/Jcli-D-11-00258.1

Tompkins, A. M., & Semie, A. G. (2017). Organization of tropical convection in low vertical wind shears: Role of updraft entrainment. *Journal of Advances in Modeling Earth Systems*, *9*, 1046–1068. https://doi.org/10.1002/2016MS000802

Weger, R. C., Lee, J., Zhu, T., & Welch, R. M. (1992). Clustering, randomness and regularity in cloud fields: 1. Theoretical considerations. *Journal of Geophysical Research*, *97*, 20,519–20,536. https://doi.org/10.1029/92JD02038

White, B. A., Buchanan, A. M., Birch, C. E., Stier, P., & Pearson, K. J. (2018). Quantifying the effects of horizontal grid length and parameterized convection on the degree of convective organization using a metric of the potential for convective interaction. *Journal of the Atmospheric Sciences*, *75*(2), 425–450. https://doi.org/10.1175/jas-d-16-0307.1

Windmiller, J. M., & Craig, G. C. (2019). Universality in the spatial evolution of self-aggregation of tropical convection. *Journal of the Atmospheric Sciences*, *76*(6), 1677–1696. https://doi.org/10.1175/Jas-D-18-0129.1

Wing, A. A., & Cronin, T. W. (2016). Self-aggregation of convection in long channel geometry. *Quarterly Journal of the Royal Meteorological Society*, *142*(694), 1–15. https://doi.org/10.1002/qj.2628

Zipser, E. J. (1977). Mesoscale and convective scale downdrafts as distinct components of squall-line structure. *Monthly Weather Review*, *105*(12), 1568–1589. https://doi.org/10.1175/1520-0493(1977)105<1568:MACDAD>2.0.CO;2